

# Ultra-Wet Operation of a Hydrogen Fueled GT Combustor: Large Eddy Simulation Employing Detailed Chemistry

O. Krüger\*, C. Duwig\*\*, S. Terhaar\* and C. O. Paschereit\*  
Corresponding author: o.krueger@tu-berlin.de

\* Chair of Fluid Dynamics, Technische Universität Berlin, Germany.

\*\* Division of Fluid Mechanics, Lund University, Sweden.

**Abstract:** Produced from renewable energy sources, hydrogen and hydrogen-rich fuels offer the possibility to overcome severe constraints on greenhouse gas emissions. Operating a gas turbine with hydrogen, however, is a challenging task. Since hydrogen is highly flammable, has a low auto-ignition temperature and due to high burning velocities, a high risk of flashbacks. Moreover, hydrogen oxidation is a highly exothermic reaction, leading to high peak temperatures and, hence, to high  $\text{NO}_x$  emission. A promising way is to add steam directly into the combustion process. Such Humidified Gas Turbines (HGT) offer the attractive possibility of increasing the plant efficiency without the cost of an additional steam turbine, as is the case for a combined gas-steam cycle. In addition to efficiency gains, adding steam into the combustion process reduces  $\text{NO}_x$  emissions.

The effect of steam on the combustion process is addressed using detailed chemistry. In order to identify an adequate oxidation mechanism, several candidates are identified and compared. The respective performances are assessed based on laminar premixed flame calculations under dry and wet conditions, for which experimentally determined flame speeds are available. Further insight is gained by observing the effect of steam on the flame structure. Moreover, the mechanism is used for the simulation of a turbulent flame in a generic swirl burner fed with hydrogen and humidified air. Large Eddy Simulations (LES) are employed. The performances of two combustion closures (ILES & TFM) and the grid sensitivity are assessed. It is shown that by adding steam, the heat release peak spreads, the flame front thickens and the flame extends further downstream. The dynamics of the oxidation layer under dry and wet conditions is captured, thus, an accurate prediction of the velocity field, flame shape and position is achieved. The latter is compared with experimental data (PIV and  $\text{OH}^*$  chemiluminescence). The reacting simulations were conducted under atmospheric conditions. The steam-air ratio was varied from 0% to 50%.

*Keywords:* Reactive Flows, Hydrogen Combustion, Diluted Flames, Large Eddy Simulation, Implicit LES, Thickened Flame Model.

## Nomenclature

– Spatial filter	$\tau_{ij}$ Stress tensor	$S_{eff}$ Effective swirl number
$\sim$ Density weighted filter	$\tau_{ij}$ Subgrid scale stress tensor	$S_L$ Laminar burning velocity
$ \cdot $ Magnitude	$\Xi$ Flame wrinkling	$t$ Time
$\varepsilon_{ijk}$ Levi-Civita symbol	$B$ Preexponential constant	$u'$ Velocity fluctuation
$\chi$ Exponent	$c$ Molar concentration	$u_0$ Bulk velocity
$\Delta$ Filter width	$D$ Diffusion coefficient	$u_\Delta$ Subgrid velocity fluctuation
$\delta_L^0$ Thermal thickness	$D_h$ Hydraulic diameter	$u_i$ Velocity component
$\lambda_f$ Taylor length scale	$D_{th}$ Thermal diffusivity	$u_{in}$ Inlet velocity
$\mu$ Dynamic viscosity	$E$ Efficiency function	$U_{s,t}$ Degree of unmixedness
$\mu_t$ Eddy viscosity	$F$ Flame thickening factor	$x$ Spatial coordinate
$\Omega$ Steam content	$F_i$ Volume force	$Y$ Mass fraction
$\omega$ Reaction rate	$h$ Specific enthalpy	$C_s$ Smagorinsky constant
$\Phi$ Equivalence ratio	$J$ Laminar diffusive flux	$Pr$ Prandtl number
$\varrho$ Density	$p$ Pressure	$Re$ Reynolds number
$\sigma$ Variance of concentration	$S_{th}$ Swirl number	

## 1 Introduction

Surrogating commonly used fossil fuels for gas turbines with carbon-free energy carriers like hydrogen are likely to play an important role in future power generation. Produced from renewable energy sources, they offer the possibility to overcome severe constraints on greenhouse gas emissions. Operating a gas turbine with hydrogen is, however, a challenging task. Since hydrogen is highly flammable, has a low autoignition temperature and due to high burning velocities, a high risk of flashbacks. In addition, hydrogen oxidation is a highly exothermic reaction, leading to high peak temperatures and, hence, to high  $\text{NO}_x$  emission.

This paper addresses the possibility to burn hydrogen in heavy-duty gas turbine applications by adding steam directly into the combustion process. Such Humidified Gas Turbines (HGT) offer the attractive possibility of increasing the plant efficiency without the need of an additional steam turbine, as is the case for combined cycles. In addition to efficiency gains, the addition of steam into the combustion process reduces  $\text{NO}_x$  emissions. It increases the specific heat capacity and thus lowers the peak temperature and the oxygen concentration. Supplementary to the thermodynamic influence of the steam on the combustion process, it alters the  $\text{NO}_x$  formation pathways. Even at constant adiabatic flame temperatures it was observed, that  $\text{NO}_x$  is reduced with increasing humidity [1, 2]. In addition, steam injection allows operation with a variety of fuels, including hydrogen and hydrogen-rich fuels. Therefore, ultra-wet GT operation is an attractive solution for industrial application.

Several humidified gas turbine cycles were analyzed by Jonsson and Yan [3]. Furthermore, investigations on humidified combustion processes with methane and a steam-air ratio of up to 5% were carried out by Bianco [4] and Guo [5].

There is extensive literature concerning hydrogen/oxygen and hydrogen/air flames. A comprehensive review over laminar flame speeds was given by Ó Conaire et al. [6]. The outcome of their investigation was

that the flame speed measurements of Dowdy et al. [7] and Tse et al. [8] can be considered to be the most representative and accurate of the entire available data set. Even though a large body of literature exists concerning hydrogen combustion, only relatively few studies were conducted on steam diluted hydrogen flames. Early studies by David et al. [9] revealed that steam diluted flame temperatures are lower than for dry flames. A survey by Kuehl [10] reported that replacing  $N_2$  with steam in low-pressure hydrogen/air flames leads to an increase of the laminar burning velocity. He claimed that the substitution with steam accelerates the combustion process by increasing the radiative heat transport from the hot products to the fresh gases. Levy [11] and Dixon-Lewis [12] offered an interpretation based on chemical kinetics for this effect. Liu et al. [13] measured the burning velocity with a laminar nozzle burner up to steam fractions of 15% and derived a correlation for the burning velocity. In the study by Koroll and Mulpuru [14], the burning velocity was examined in a similar experiment with molar steam fractions up to 50%. They concluded that steam does not act as an inert diluent. To our knowledge, this is the most comprehensive investigation on hydrogen flames concerning high steam contents. More recent work on hydrogen diluted flames was done by Kwon and Faeth [15], and Kuznetsov [16]. Kwon and Faeth reported on experimentally obtained laminar flame speeds for  $N_2/He/Ar$  as diluents in freely propagating spherical flames.

Numerous reactions schemes including a detailed  $H_2/O_2$  subset can be found in the literature. A comprehensive overview was given by Ströhle and Myhrvold [17]. They assessed the performances of several mechanisms for different criteria such as ignition delay, burning velocity and pressure dependence with experimental data. They concluded that the mechanism of Li [18] is the most suitable. The mechanism is based on previous publications by the group of F. L. Dryer at Princeton University. Recently Burke updated the mechanism of Li [19]. He improved it further and validated it against a wide range of experimental conditions. Le Cong and Dagaut [20] developed a reaction mechanism focused on oxidation of nitrogen diluted syngas compositions ( $H_2/CO/CH_4$ ). The scheme is very comprehensive and consists of 128 species and 924 reversible reactions. It showed good agreement with experimental data. The mechanism of the CRECK Modeling Group was published [21] recently. It is modularly built and features prompt and thermal  $NO_x$  formation pathways.

The specific objective of this study is the investigation of the premixed combustion of pure hydrogen diluted with varying amounts of steam. The effect of steam on the combustion process is addressed by employing detailed chemistry. One aim of this study is to identify an adequate detailed reaction mechanism. Several candidates are identified and compared employing one-dimensional laminar premixed flame computations at several steam levels for which experimentally determined flame speeds are available.

The reaction mechanism is then used for simulating a turbulent flame in a generic swirl burner using Large Eddy Simulations (LES). Turbulent combustion is a complex topic, which involves non-linear multi-scale phenomena. Consequently, the flame location is unsteady in nature and very sensitive to perturbations. To present a suitable simulation strategy for handling wet combustion, two different combustion closures are investigated and the grid sensitivity is assessed. To investigate the influence of steam on the combustion process simulations with different steam contents are carried out and are compared to experimental data. The reacting simulations will be conducted under atmospheric conditions and the steam-air ratio was varied from 0% to 50%.

Firstly, the investigated geometry and the experimental and numerical techniques are presented. Secondly, an adequate detailed reaction mechanism is identified by performing one-dimensional laminar premixed flame calculations. Afterwards, the mechanism is used for LES to assess the influence of the grid resolution as well as the chosen combustion closure. The influence of different steam contents on the combustion processes is assessed employing LES. Velocity profiles, flame shape and positions are compared to  $OH^*$  chemiluminescence recordings and PIV measurements. Finally, the results are summarized and conclusions are drawn.

## 2 Investigated Configuration

The simulations were conducted on an unscaled cylindrical domain with an attached swirl generator, as shown in Figure 1. The domain is adopted from the experimental setup. Due to limited computational resources the length of the combustion chamber was truncated. As a characteristic length and velocity to be the hydraulic diameter of the burner outlet  $D_h = 20.0$  mm and the mean bulk velocity  $u_0$  at the burner exit were chosen.

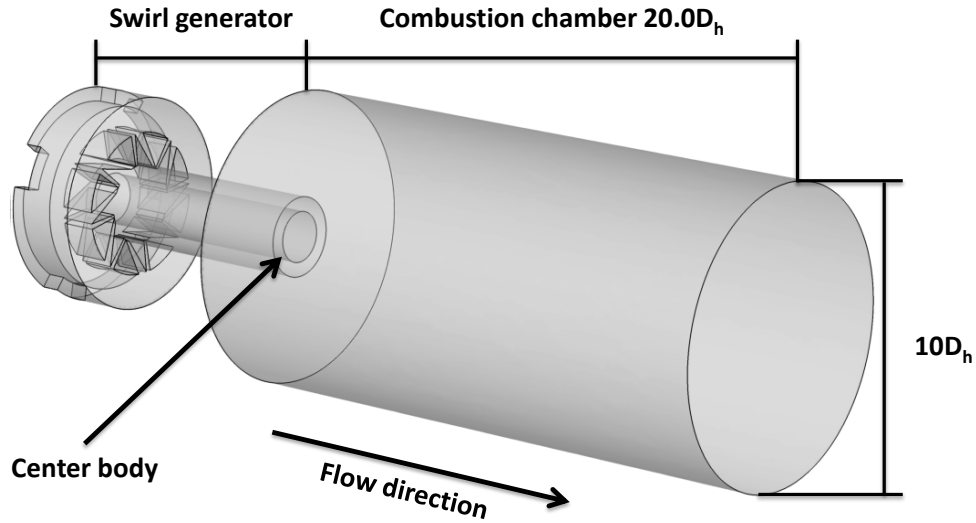


Figure 1: Schematic drawing of the computational domain

The swirl burner (MOVABLE BLOCK BURNER) consists of eight movable and eight fixed alternately placed blocks as shown in Figure 2. By simultaneously rotating the movable blocks about the symmetry axis the swirl intensity can be altered. This yields modulation of the swirl intensity between 0 and 2, but as mentioned above a constant swirl number of  $S_{th} = 0.7$  was used in the present study. The main gas flow consists of an adjustable amount of air and steam and is premixed before entering the swirl generator. Fuel, in this case hydrogen, is injected at the bottom plate of the swirl generator through 16 holes. In previous investigations the spatial and temporal degree of unmixedness of the air-fuel mixture was addressed [22]. The degree of unmixedness is defined as  $U_{s,t} = \sigma_{s,t}^2 / \bar{c}(1-\bar{c})$ , where  $\sigma_{s,t}$  is the temporal (subscript  $t$ ) or spatial (subscript  $s$ ) variance of concentration fluctuations and  $\bar{c}$  is the mean molar fuel concentration. It was found that the spatial and temporal degree of unmixedness was of the order of  $10^{-4}$ . Thus, the air-steam-fuel composition is regarded as technically premixed. This has been taken into account for the simulations by directly applying the air-steam-fuel composition to the inlet, without considering the mixing process.

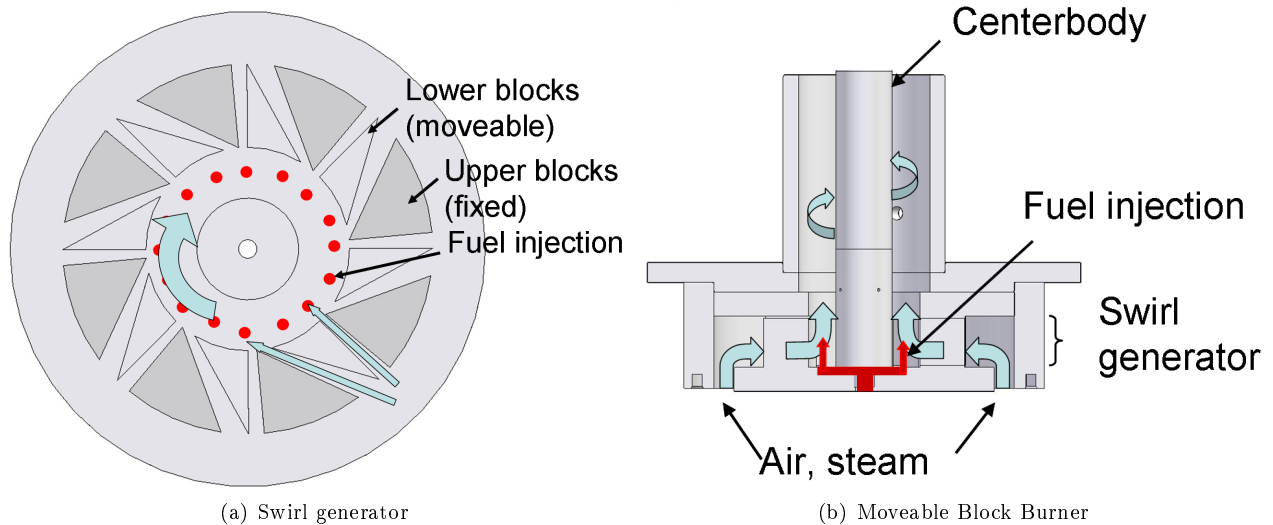


Figure 2: Swirl generator and Moveable Block Burner

### 3 Experimental Techniques

The reacting flow measurements were performed in a gas-fired test rig under atmospheric conditions. The burner was fired with hydrogen, and the air was preheated and mixed with overheated steam before entering the burner.

To provide optical access, the combustion chamber consists of a cylindrical silica glass followed by a water-cooled exhaust tube. The optical access allows for the application of Particle Image Velocimetry (PIV). For the PIV measurements, aluminum oxide particles of a nominal diameter of  $1\ \mu\text{m}$  were seeded into the flow upstream of the swirl generator using a fluidized bed seeding generator. The flame position was assessed by recording its OH\* chemiluminescence using an ICCD camera. In order to recover the radial intensity distribution the images were decomposed applying an inverse Abel transformation according to [23]. The combustor inlet temperature was measured in the mixing tube upstream of the burner outlet. Further information on the experimental setup is provided in [24].

### 4 Operating Conditions

In order to assess the influence of steam on the combustion process, three cases were conducted. The first case was computed with the absence of steam at ambient temperature and lean conditions, and will be denoted in the following as “dry”. The two other cases were carried out with moderate and high steam content and are referred to “moderate-wet” and “ultra-wet” in the following. The steam content  $\Omega = \dot{m}_{steam}/\dot{m}_{air}$  is defined as the ratio of the mass flow rate of steam  $\dot{m}_{steam}$  to the mass flow rate of air  $\dot{m}_{air}$ . In addition, the respective performances of two combustion models were assessed, as well as the grid sensitivity.

One objective of this survey is to show that adding steam directly into the combustion process allows for hydrogen combustion at realistic gas turbine conditions, with regards to the turbine inlet temperature ( $\approx 1643\ \text{K}$ ).

During the experiments, the total mass flow rate of air plus steam was kept constant. The swirl number was adjusted to  $S_{th} = 0.7$  to assure vortex breakdown in the combustion chamber. The operation conditions are summarized in Table 1.

Table 1: Operating Conditions

Condition		Case 1 (Dry)	Case 2 (Moderate-Wet)	Case 3 (Ultra-Wet)
Inlet velocity	$u_{in}$	14.94 m/s	26.55 m/s	38.89 m/s
Bulk velocity	$u_0$	34.71 m/s	61.65 m/s	88.37 m/s
Pressure	$p$	101,325 Pa	101,325 Pa	101,325 Pa
Reynolds number	$Re$	39,000	31,000	26,000
Steam content	$\Omega$	0%	20%	50%
Equivalence ratio	$\Phi$	0.5	0.6	0.75
Inlet temperature	$T_u$	293 K	463 K	633 K
Adiabatic flame temperature	$T_{ad}$	1643 K	1623 K	1643 K

### 5 Numerical Methods and Subgrid Scale Modeling

The motion of a reacting flow is described by balance equations of momentum, mass, species and energy. In LES a “low-pass” filter is applied to the dependent variables, and thus removes the dependence on the small eddy scales, so that the equations only describe the larger turbulent fluctuations [25, 26]. This results in unclosed terms, usually referred as the subgrid scale (SGS). Applying filtering to the balance equations leads to the Favre averaged filtered equations, which reads as follows:

Continuity:

$$\frac{\partial \bar{\varrho}}{\partial t} + \frac{\partial \bar{\varrho} \tilde{u}_j}{\partial x_j} = 0. \quad (1)$$

Momentum ( $i = 1, 2, 3$ ):

$$\frac{\partial \bar{\varrho} \tilde{u}_i}{\partial t} + \frac{\partial (\bar{\varrho} \tilde{u}_j \tilde{u}_i)}{\partial x_j} = - \frac{\partial}{\partial x_j} [\bar{\varrho} (\widetilde{u_i u_j} - \tilde{u}_i \tilde{u}_j)] - \frac{\partial \bar{p}}{\partial x_i} + \frac{\partial \bar{\tau}_{ij}}{\partial x_j} + \bar{F}_i. \quad (2)$$

Here, the superscripts  $-$  and  $\sim$  denote filtered and Favre filtered quantities, rather than ensemble means. In addition,  $u_i$  is the velocity component,  $\varrho$  the density,  $p$  the pressure,  $\mu$  the dynamic viscosity,  $F_i$  a volume force and  $\tau_{ij}$  is an unclosed term, usually denoted as the subgrid scale stress tensor.

The mass conservation equation for chemical species  $k$  is described as follows:

$$\frac{\partial \bar{\varrho} \tilde{Y}_k}{\partial t} + \frac{\partial}{\partial x_i} (\bar{\varrho} \tilde{u}_i \tilde{Y}_k) = \frac{\partial}{\partial x_i} [\bar{J}_i^k \tilde{Y}_k - \bar{\varrho} (\widetilde{u_i Y_k} - \tilde{u}_i \tilde{Y}_k)] + \bar{\omega}_k, \quad (3)$$

where  $Y_k$  is the mass fraction of the species  $k$ ,  $\omega_k$  is the reaction rate and  $J_i^k$  is the  $i$ -component of the laminar diffusive flux of species  $k$ . For the conservation of energy, the enthalpy balance equation is employed, where a low Mach assumption is regarded:

$$\frac{\partial \bar{\varrho} \tilde{h}_t}{\partial t} + \frac{\partial \bar{\varrho} \tilde{u}_i \tilde{h}_t}{\partial x_i} = \frac{\partial}{\partial x_i} \left( \frac{(\mu_t + \mu)}{Pr} \frac{\partial \tilde{h}_t}{\partial x_i} \right). \quad (4)$$

Here,  $h_t = h + u_i u_i / 2$  is the total enthalpy and can be described by the specific enthalpy  $h$ .  $\mu$  denotes the dynamic viscosity of the fluid,  $\mu_t$  the eddy viscosity and  $Pr = 0.7$  the Prandtl number. Regarding a low Mach approximation results in an additional simplified equation of state, where the density is a function of the temperature and the composition only.

The filtering is assumed to be a linear function, and therefore, to be commutative with temporal and spatial derivatives. This assumption is not valid for non-linear terms and cannot be described by filtered variables. Hence, they are gathered on the right-hand side. These terms, collectively denoted as subgrid scale (SGS) terms, are unclosed and must be modeled. In the present study, the SGS term is modeled by the classical Smagorinsky approach [27]. In this approach, the unresolved stress tensor  $\tau_{ij} = \bar{\varrho} \widetilde{u_i u_j} - \bar{\varrho} \tilde{u}_i \tilde{u}_j$  is modeled by the Boussinesq hypothesis, in which the effect of the unresolved turbulence on the large-scale flow is considered as an increase in viscosity. The filter length scale is the cubic root of the local grid cell volume. The Smagorinsky constant  $C_s$  was set to  $C_s = 0.1683$ .

The simulations have been carried out employing the open-source platform OpenFOAM. In order to handle the combustion process at wet conditions, a customized solver for low Mach number reacting flows was used [28, 29, 30]. For both cases, the pressure velocity coupling is performed applying the PISO algorithm as described by [31], ensuring that continuity is satisfied. For all spatial derivatives, except for the convective terms in the enthalpy and the mass fraction equations, second order differencing is used. These convective terms are treated using a second order accurate total-variation-diminishing (TVD) scheme for avoiding non-physical over-shoots. Time derivatives are treated applying a second order upwind scheme and time integration is done implicitly in a sequential manner. Dirichlet boundary conditions are enforced at the inlet for all variables except for the pressure, which uses a zero-gradient condition (Neumann). Similarly, the out flow is treated using zero-gradient for all variables. Non-slip walls (zero velocity) are used with zero gradient for the other variables except for the temperature, for which a constant wall temperature was set.

## 6 Combustion Modeling

### One-Dimensional Flame Modeling

One-dimensional computations were assessed using the open-source software CANTERA in order to analyze the influence of steam on the combustion process. The software includes important effects for hydrogen combustion, as thermal diffusion and multicomponent diffusion. For only one dimension, the governing equations for energy and mass fractions are reduced to a system of ODEs (Ordinary Differential Equations) in the axial coordinate. By applying finite-differences a system of nonlinear algebraic equations is formed from the flow. The numerical method is based on a hybrid Newton/time-stepping algorithm to solve the equations. The grid was adaptively refined/coarsened to ensure sufficiently resolved gradients, since the largest source of errors is the spatial discretization.

In the study of Ströhle and Myhrvold [17] several reaction mechanisms for H<sub>2</sub>/O<sub>2</sub> and H<sub>2</sub>/air combustion were evaluated and they concluded that the mechanism of Li [18] would be the most suitable mechanism for flame prediction. The reaction scheme was recently updated by Burke [19] with the primary objective to incorporate recent improvements in rate constants, especially for diluted and high-pressure flames. Due to these improvements this model was employed in the present study, even if elevated pressures are not considered. The model consists of 13 species and 27 reactions and was validated using the data by Li [18].

In addition two representatives of C1/C2 species oxidation were considered, since both are based on a detailed H<sub>2</sub>/O<sub>2</sub> subset. The first of them was published by Le Cong and Dagaut [20] and contains 128 species and 924 reversible reactions overall. The H<sub>2</sub> oxidation subset is represented by 12 species and 22 reactions. The second mechanism is from the CRECK Modeling Group [21]. For this scheme the H<sub>2</sub>/O<sub>2</sub> subset consists of 32 Species and 174 Reactions.

Additionally, the GRI-Mech 3.0 [32] (26 reversible reactions for H<sub>2</sub>/O<sub>2</sub> kinetics) is also included, since it is used as a reference by many researchers.

Based on their respective performance, LES simulations were conducted employing the most suitable reaction mechanism. Since none of the aforementioned mechanisms features the formation of OH\*, all models were extended by OH\* formation pathways according to Smith [33]. This includes one additional species (OH\*) and 7 reactions.

### Reaction Modeling

Incorporating combustion chemistry into LES involves finding a suitable reaction mechanism and solving the filtered species equations. An additional modeling issue lies in the filtered species equations, which contain the filtered reaction rates  $\bar{\omega}$ . The reaction rates are non-linear functions of species concentration and temperature. Different avenues have been used for modeling of the filtered reaction rate, starting by extending Reynolds-Averaged Navier-Stokes (RANS) combustion models to LES applications. Recently modern methods have been proposed that were specifically designed for the LES framework [25].

Examples of such methods include (i) Implicit LES (ILES), [34, 35, 36], (ii) Thickened Flame Models (TFM) [37, 38, 25], (iii) Linear Eddy Models (LEM) with embedded 1D grids [39], (iv) Flamelet Models (FM) [40, 41, 42], (v) Eddy Dissipation Concept (EDC) [43], (vi) Partially Stirred Reactor (PaSR) [34] and (vii) Filtered Density Function (FDF) models [44, 35]. While the methods (iv-vi) have a counter-part in the RANS framework, the methods (i-iii) are solely valid for LES applications.

The investigated flame in the present paper is characterized by a relatively high Karlovitz number as a large amount of steam is added to the reactants, which spreads the heat release peak. The Karlovitz number can be calculated as

$$Ka \sim \left( \frac{u'}{S_L} \right)^{\frac{3}{2}} \left( \frac{D_h}{\delta_L^0} \right)^{-\frac{1}{2}}, \quad (5)$$

where  $u'$  is the velocity fluctuation,  $S_L$  the laminar flame velocity and  $\delta_L^0$  the flame thickness. The Damköhler number can be determined similarly:

$$Da \sim \frac{D_h/u'}{\delta_L^0/S_L}. \quad (6)$$

The calculations of  $Ka$  and  $Da$  for different steam levels is listed in Table 2. The velocity fluctuation  $u'$

was calculated from incompressible LES. The thermal thickness  $\delta_L^0$  and the laminar flame velocity  $S_L$  were calculated with the one-dimensional approach mentioned above.

Table 2: Karlovitz and Damköhler number for the three considered cases

Condition		Case 1 (Dry)	Case 2 (Moderate-Wet)	Case 3 (Ultra-Wet)
Steam content	$\Omega$	0%	20%	50%
Equivalence ratio	$\Phi$	0.5	0.6	0.75
Laminar burning velocity	$S_L$	0.5 m/s	0.78 m/s	0.33 m/s
Thermal thickness	$\delta_L^0$	$4.4 \cdot 10^{-4}$ m	$4.8 \cdot 10^{-4}$ mm	$5.6 \cdot 10^{-4}$ mm
Flame thickening factor	$F$	2.1	2.1	2.1
Karlovitz number	$Ka$	7.76	9.6	8.43
Damköhler number	$Da$	3.2	2.6	2.6

With such a high Karlovitz and Damköhler number, the turbulent integral scale is larger than the chemical time scale. Thus, the Kolmogorov scales are smaller than the flame thickness and the inner flame structure may be affected. This flame regime is well known as the “thickened flame regime” or “distributed reaction zone” [25]. Therefore, the flame is definitely subject to strong finite rate chemistry effects and suitable candidates for resolving this effect are ILES, TFM, LEM, EDC, PaSR and FDF. LEM and transported FDF are very CPU intensive techniques when used with LES, while presumed FDF and ILES keep the CPU costs at reasonable levels. EDC and PaSR have intermediate CPU cost, though potentially important when dealing with complex burner geometries. The present study focus on using ILES and TFM, which have the attractive feature of handling complex chemistry naturally and with reasonable extra cost.

### Implicit LES

The Implicit LES (ILES) (also sometimes referred to Monotonically Integrated LES - MILES) closure computes directly the reaction rate of the  $k$ -th species through an Arrhenius expression. According to [34, 35, 36] the filtered reaction terms for species  $j$  are given by:

$$\overline{\dot{\omega}_j(Y_i, T)} = \dot{\omega}_j(\tilde{Y}_i, \tilde{T}) . \quad (7)$$

The assumption leading to ILES corresponds to the assumption that each cell is a perfectly-stirred reactor, and thus that the subgrid mixing is faster than chemical reactions. Therefore, a very intense subgrid mixing is required to ensure that the filter box, or LES grid cell, is homogeneous.

An alternative measure is the thickening factor  $F$  used in the Thickened Flame Model (TFM). The factor  $F$  is usually computed in order to be able to resolve the flame front on 3 – 5 grid points:

$$F \sim 3\Delta/\delta_L^0 , \quad (8)$$

where  $\Delta = 4 \cdot 10^{-4}$  mm represents a characteristic element size in the shear layer. Usually  $F$  is less sensitive than the local Damköhler number  $Da$ , as it does not account for the subgrid stirring, though the ILES domain of validity corresponds to  $F$  close to or below 3. The calculations of  $F$  for the three cases as listed in Table 2 indicates that the present flame falls well into the domain of validity of ILES and the reaction brush is indeed resolved on the LES grid.

Equation (7) would fail in the RANS framework, but is valid for laminar flow simulation and direct numerical simulation (DNS). The validity of Equation (7) with LES depends on the relative grid resolution and also on the subgrid physics. Although using a typical LES-grid, far from DNS, Equation (7) was shown to approximate the reaction rate reasonably well, as reported in [45, 46, 34, 35]. These studies suggest that ILES is an eligible approach for combustion simulation and that it may perform equally well compared to other closures.

### Thickened Flame Model

The Thickened Flame Model (TFM) [37, 47, 38, 25, 48], originally proposed by Butler and O'Rourke [37], is a well established closure. It artificially thickens the flame front, in order to resolve the flame front on the LES grid. Based on the laminar theory [25] the flame speed and thickness can be expressed as:

$$S_L \sim \sqrt{D_{th}B}; \quad \delta_L^0 \sim \frac{D_{th}}{S_L} = \sqrt{\frac{D_{th}}{B}}, \quad (9)$$

where  $D_{th}$  is the thermal diffusivity and  $B$  the preexponential constant. By multiplying the thermal diffusivity, and simultaneously dividing  $B$  with the same factor  $F$ , the flame speed keeps constant, while the flame thickness is artificially increased. However, this also decreases the Damköhler number by the factor of  $F$ . In order to correct this Colin et al. [47] introduced an efficiency function  $E$ , which takes the subgrid wrinkling into account to correct the unresolved features.

For the model the chemical oxidation is handled by the usage of an Arrhenius expression. The filtered scalar equations reads:

$$\overline{\dot{\omega}_k(Y_j, T)} = \frac{E}{F} \dot{\omega}_k(\tilde{Y}_j, \tilde{T}), \quad (10)$$

where  $F$  is the thickening factor and  $E$  an efficiency function. The unresolved scalar transport  $D_{TFM}$  is modeled similarly, by an effective diffusion related to the molecular diffusion coefficient  $D_i$ :

$$D_{TFM} = EFD_k, \quad (11)$$

From combining equation 10, 11 with equation 3 it follows the species balance for the Thickened Flame Model:

$$\frac{\partial \bar{\rho} \tilde{Y}_k}{\partial t} + \frac{\partial}{\partial x_i} (\bar{\rho} \tilde{u}_i \tilde{Y}_k) = \frac{\partial}{\partial x_i} \left[ \bar{\rho} EFD_k \frac{\partial \tilde{Y}_k}{\partial x_i} \right] + \frac{E}{F} \dot{\omega}_k(\tilde{Y}_j, \tilde{T}). \quad (12)$$

The efficiency function  $E \propto \Xi$  is modeled with concern to the flame wrinkling  $\Xi$  that is taken into account by the fractal flame wrinkling approach (FFW) of Fureby [49]. The flame thickening is only needed where the flame is present, and therefore  $E$  is restricted to a minimal value of 1:

$$E \propto \Xi \propto \max \left( 1, \left[ \frac{u_\Delta}{S_L} \right]^\chi \right), \quad (13)$$

with the exponent  $\chi$  being 0.3 and the subgrid velocity fluctuation  $u_\Delta$ , which reads as:

$$u_\Delta = 2 \left| \frac{\partial^2}{\partial x_i^2} \left( \varepsilon_{ijk} \frac{\partial u_k}{\partial x_j} \right) \right| \Delta^3. \quad (14)$$

Of particular concern is the thickening factor  $F$ , which is usually computed on 3 – 5 grid points [36]. In addition the flame thickening is only necessary where the flame is present to ensure that  $F = E = 1$ , which is formally identical to the ILES closure. Besides, the thickening factor  $F$  is an indicator of the ILES closure, which complements the local Damköhler and Karlovitz number. As a consequence  $F$  may be computed in advance to a simulation and hence serve as an indicator for the validity of ILES. Since,  $F$  does not hold information related to turbulence intensity,  $F$  may be considered as a necessary but not adequate indicator of the potential validity of ILES.

A more refined version of the Thickend Flame Model has been reported by [48], where the flame thickening factor  $F$  is computed dynamically.

## 7 Numerical Setup

As listed in Table 3 six computations were carried out with Reynolds numbers between  $Re \approx 39,000$  and  $Re \approx 67,000$ . In order to investigate the grid dependence two grids were used. Two computational grids are used in the present study, both consisting of unstructured polyhedral cells with refinement towards the inner shear layer of the inner recirculation zone, ensuring that the smaller cells are located where scalar and velocity gradients are expected to be large. For the *finer* mesh the grid resolution was almost doubled in the flame zone. The *coarser* grid contains 1.1 million cells (3.9 millions nodes) compared to 2.1 millions (11.3 millions nodes) on the *finer* mesh. For the *coarser* mesh this resulted in a Taylor turbulent length scale of  $\lambda_f$ :

$$\overline{\left(\frac{\partial u_{ax}}{\partial x}\right)^2} = \frac{2u'^2}{\lambda_f^2} \approx 0.08D_h. \quad (15)$$

Hence, the smallest resolved scales are in the inertial range of the turbulent spectrum and the grid is suitable for performing LES. The second grid was refined in the area of the inner shear layer. Both meshes were used to perform a grid sensitivity study with ILES as combustion closure at dry conditions according to Table 1. Moreover, a detailed grid sensitivity study was performed and reported earlier in [50] showing that the refining in the present grid does not change the mean and RMS fields significantly.

As aforementioned, due to limited computational resources the length of the combustion chamber was truncated. Terhaar and coworkers [51] reported that for an effective swirl number  $S_{eff} \leq 0.3$  the flow can be considered to be supercritical, and thus, has the outlet a negligible influence on the upstream flow field. The effective swirl number  $S_{eff}$  can be expressed by:

$$S_{eff} = S_{th} \frac{T_u}{T_b}, \quad (16)$$

where  $T_u/T_b$  denotes the temperature ratio obtained using calculated flame temperature  $T_b$  and inlet temperature  $T_u$ . With a theoretical swirl number of  $S_{th} = 0.7$  and the temperatures listed in Table 1 a maximum effective swirl number of  $S_{eff} = 0.26$  can be determined, and thus, the flow can be considered supercritical.

In addition to the grid study the performances of the ILES were compared to the TFM combustion closure for different values of  $F$ . Furthermore, the influence of steam was assessed with several steam levels.

In addition to the operating conditions as listed in Table 1, a wall temperature ( $T = 900$  K) was set for the walls of the combustion chamber, since it was observed in previous investigations [28, 29] that heat losses through the walls have a major impact on the flame prediction. The wall temperature was derived from experiments.

Table 3: Presentation of the six considered cases

Case	Name	Equivalence ratio $\Phi$	Steam content $\Omega$	Combustion Closure	Mesh
I	ILES ( $\Omega = 0.0$ )	0.5	0.0	ILES	coarse
II	ILES fine	0.5	0.0	ILES	fine
III	TFM F=1.5	0.5	0.0	TFM	coarse
IV	TFM F=2.1	0.5	0.0	TFM	coarse
V	ILES $\Omega = 0.2$	0.6	0.2	ILES	coarse
VI	ILES $\Omega = 0.5$	0.75	0.5	ILES	coarse

## 8 Results and Discussion

### One-Dimensional Flame Analysis

The laminar burning velocity is a key parameter in characterizing a combustible mixture. Hence, the comparison of calculated flame speeds with corresponding measurements is of particular concern. The laminar burning velocity ( $S_L$ ) is defined as the local velocity at which the flame front propagates normal to itself into the unburned gas. It depends primarily on the pressure, temperature and the composition. As the number of studies concerning steam diluted hydrogen flames with high amounts of steam is still very limited, the following analysis refers to the experimental data published by Koroll and Mulpuru [14]. They investigated  $H_2$ /air/steam compositions up to molar fractions of 50% steam at ambient pressure. Burning velocities were measured with a nozzle burner applying the Schlieren cone angle method and particle tracking with Laser Doppler Anemometry. The experiments with  $H_2$ /air/steam compositions were conducted at an inlet temperature of 373 K and a burner diameter of 5 mm. The crucial effect of flame curvature was evaluated with different diameters and Koroll [14] and the data was corrected subsequently. In the study the overall accuracy was not given, but Edmondson [52] reported a relative error of less than  $\pm 5\%$  for a similar configuration. Calculations of the laminar burning velocity in a one-dimensional freely propagating flame were performed using four different reaction schemes. The mechanisms of Burke [53], Dagaut [20], the CRECK Modeling Group [21] and the GRI 3.0 [32] were compared to the measurements of Koroll.

In Figure 3 the results are given for the burning velocity of  $H_2$ /air/steam compositions at 373 K. Error bars according to [52] are provided for steam levels of 0% and 12%. In the absence of steam all four mechanisms are generally in good agreement with the measurements. With raising steam contents the deviations between the reaction schemes and the measurements become more apparent. Especially the CRECK and GRI mechanisms tend to underpredict the burning velocity at rich conditions and high steam levels. On the contrary the Dagaut and Burke mechanism predict similar results that are well in line with the measurements. Even with high steam contents both mechanisms are close to the experimental data, but the Dagaut mechanism tends to slightly underestimate the flame velocity. In the absence of steam, the GRI mechanism predicts a slightly faster maximum flame speed. With increasing steam ratios and hydrogen content, the burning velocity is under estimated.

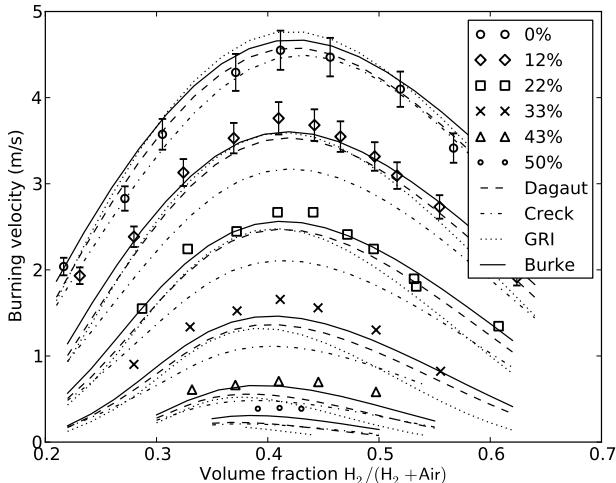


Figure 3: Laminar burning velocity of hydrogen at 1 atm and  $T_u = 373$  K for different steam levels and reaction mechanisms. Comparison between experimental data (symbols) and model predictions (lines). Experimental data according to Koroll [14].

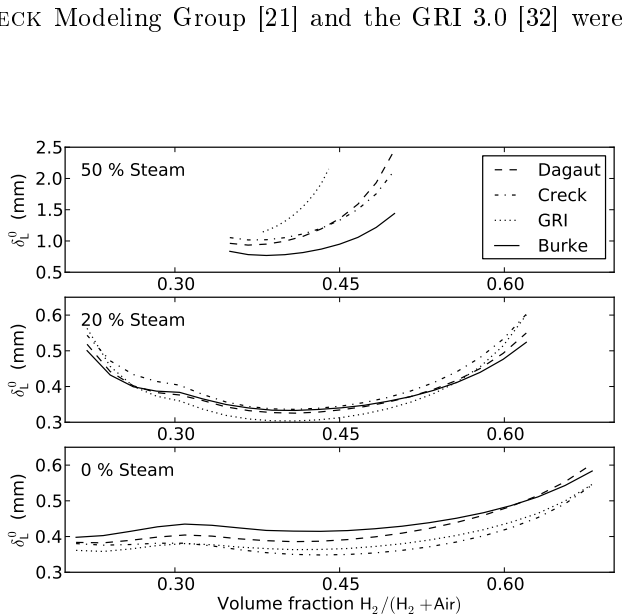


Figure 4: Thermal thickness  $\delta_L^0$  of a hydrogen/air/steam flame at 1 atm and  $T_u = 373$  K for different steam contents and reaction schemes.

The thermal thickness is a well suited measure and an obvious requirement for numerical combustion simulations, since it controls the required mesh resolution. For most combustion modeling approaches the flame structure must be resolved by enough grid points, in order to resolve the gradients sufficiently. Different definitions are available, based either on scaling laws or on one-dimensional flame calculations. According to Poinot [25], the thermal thickness  $\delta_L^0$  is the best suited definition. It requires a temperature distribution and is defined by the temperature difference of the inlet temperature  $T_u$  and the temperature of the burnt gases  $T_b$ , divided by the maximum of the temperature gradient:

$$\delta_L^0 = \frac{T_b - T_u}{\max\left(\left|\frac{\partial T}{\partial x}\right|\right)}. \quad (17)$$

Figure 4 depicts the thermal thickness as a function of the hydrogen content for different steam levels. As expected, the thermal thickness for a hydrogen flame is very thin. In the absence of steam the flame thickness increases with the hydrogen input. As shown in the figure the mechanisms show a common tendency, but differ significantly from each other. The predictions of the CRECK mechanism deviate from the Burke mechanism by about 17%. With the increase of steam, the flame thickness grows, especially in the lean ( $[H_2]/[H_2+air] \lesssim 0.3$ ) and very rich ( $[H_2]/[H_2+air] > 0.5$ ) regime. For a steam content of 20%, the C1/C2 mechanisms are close to the predictions of the Burke mechanism. With a further increase of the steam content to 50%, the C1/C2 mechanisms predict a significantly larger thermal thickness. In particular, the GRI mechanism shows a high deviation to the Burke mechanism. All calculations show a global minimum at  $[H_2]/[H_2+air] \approx 0.4$ . Here, the burning velocity reaches its maximum and, hence, explains the minimum of the thermal thickness. Without accompanying data for the thermal thickness, the reaction mechanisms cannot be ranked. However, with respect to the findings of the laminar burning velocity, it is assumed that the Burke mechanism is the most suitable mechanism for steam diluted hydrogen flames, and is therefore, used for the following analysis and the LES simulations. Since the mechanism lacks the formation of  $OH^*$  species, it was extended by the  $OH^*$  subset of Smith [54]. An influence of these extensions on the predictions on the laminar burning velocity was of course verified beforehand.

Figure 5 shows the laminar burning velocity, the thermal thickness and the flame thickening factor as a function of the steam content ( $\Omega$ ) for constant burned gas temperatures  $T_b$ . For a better comparison, calculations with methane at 1773 K conducted with the GRI mechanism are provided. As can be seen, the burning velocity depends almost linearly on the temperature  $T_b$  and decreases with raising steam content. As expected, the burning velocities for the hydrogen flames are significantly higher than those for the methane flame. In contrast to the methane flame, the thermal thickness changes only slightly with steam content for the hydrogen flame. A similar behavior may be found for the flame thickening factor  $F = 3\Delta/\delta_L^0$ , since it is only based on a characteristic length  $\Delta$  and the thermal thickness  $\delta_L^0$ . A more detailed analysis of the influence of steam on the kinetics can be found in [30].

## Large Eddy Simulations

The performed LES computations run with an adjustable time step to ensure a maximum Courant-Friedrichs-Lewy below 0.2. This resulted in an averaged time step of  $10^{-7}$ s. The results were time-averaged over 0.05 s

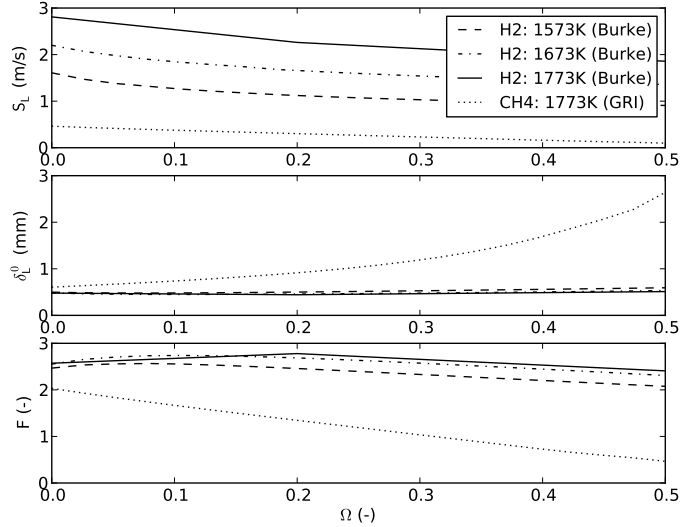


Figure 5: Steam content dependence of the laminar burning velocity (top), the thermal thickness (middle) and the flame thickening factor (bottom) at constant outlet temperatures  $T_b$ . The inlet temperature was 600 K. Model predictions were assessed with the mechanism of Burke [53] and with the GRI 3.0-Mech for methane ( $T_b = 1773$  K).

physical seconds after reaching a statistically steady state and showed a symmetrically averaged velocity field. Several cases were performed at ambient pressure to investigate the sensitivity of the grid and combustion closure as well as the influence of steam on the combustion process. The additional operating conditions were set according to Table 1 and 3.

### Sensitivity Analysis

The sensitivity of the solution to the grid resolution and the combustion closure is investigated by comparing velocity, density gradients and OH\* species concentration. Since LES is only able to resolve turbulent scales that are larger than the grid spacing. It is essential to ensure grid independence by comparison of grids with different spatial resolution.

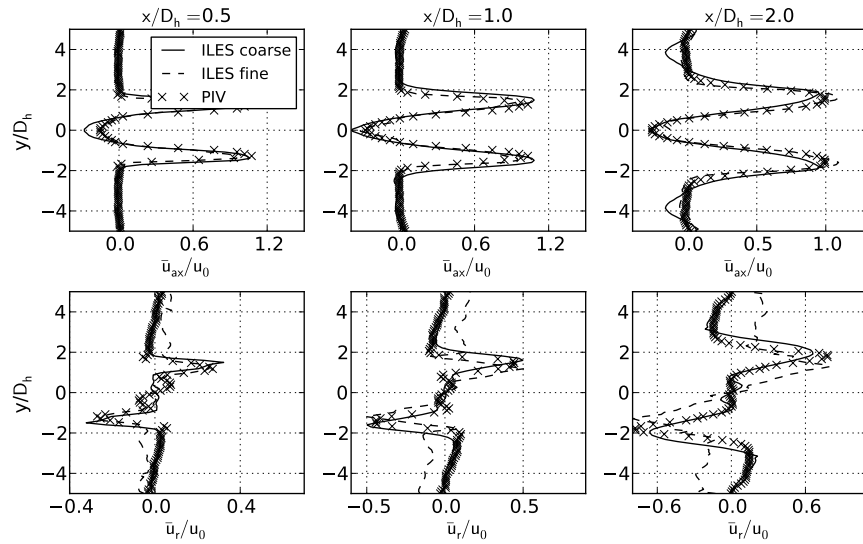


Figure 6: Mean axial and radial velocity profiles at different streamwise positions ( $x/D_h = 0.5; 1.0; 2.0$ ). Profiles are normalized by the burner exit velocity  $u_0$ .

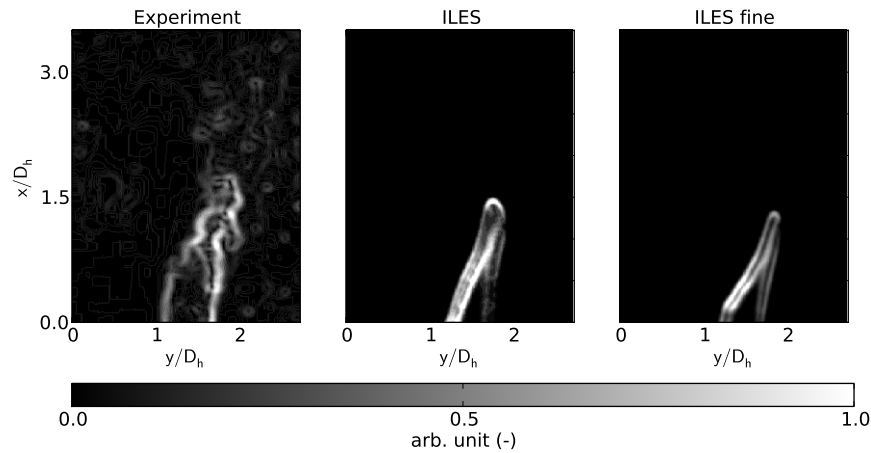


Figure 7: Visualization of the flame front. Processed PIV (left); Inverse temperature gradient of LES (middle and right).

Due to the high computational costs, it is difficult to consider large grid variations. Therefore, only two simulations were conducted. The first computation was performed with a "coarse" mesh. For the "finer"

mesh, the spatial density of the mesh was doubled in the zone where the main reactions and steep gradients were expected.

Figure 6 depicts a comparison of the measured and simulated mean axial and radial mean flow field at different axial positions. The origin ( $x/D_h = 0.0$ ) is located at the burner exit and the profiles are normalized by the burner exit velocity  $u_0$ . Near the burner exit an inner recirculation zone is established due to the vortex breakdown downstream of the sudden expansion. A shear layer is formed between the inner recirculation and the surrounding swirling flow, where high gradients are present.

The axial velocities are well in line with the measurements for the axial velocity. Near the burner exit, the negative axial velocity in the inner recirculation zone is slightly over predicted for the coarse case. Furthermore, at  $x/D_h = 2.0$ , the LES predicts the slope at the inner shear layer slightly different and an external recirculation zone, which cannot be observed in the measurements. On the one hand, this could stem from higher measurement uncertainties near the walls, for example caused by reflections or seeding residuals. On the other hand, this could indicate a too short averaging time for the computations. The prediction of the radial velocities shows for the fine case a small deviation from the measurements. As is the case for the simulations, the radial velocity should become zero at the walls. Again, the discrepancies of the experimental data can be attributed to reflections and adhesion of seeding particles near the walls. Nevertheless, both simulations show a good agreement to the measurements. By applying a Sobel filter to the PIV images the flame front shape can be deduced from the step in the particle number density caused by the steep temperature increase in the reaction zone. Pfadler and coworkers [55] as well as Tachibana et al. [56] revealed that this method, yields nearly the same spatial position as the heat release measurements, the flame front wrinkling or the steepest slope in the OH\* distribution as is the case for planar OH LIF measurements. In order to compare the simulations to the processed PIV recordings the inverse temperature gradient was used.

Figure 7 shows the Sobel filtered PIV recordings and the according LES results. As can be seen, the measurement exhibits small scales that are not predicted by the computations. Especially the wrinkling of the flame front is not predicted. However, the flame shape, position and angle are reproduced. It should be mentioned, that the small scales of the measurements are not necessarily directly linked with the density gradient, since the particles are subject to turbulence and therefore, discrepancies cannot solely be attributed to the grid resolution. Nevertheless, the differences between the simulations are small.

The flame is approximately represented by the concentration of active OH radicals. In order to compare the OH\* chemiluminescence measurements qualitatively with the computations, the recordings were transformed by an Abel inversion to give a view of the flame in a slice without losses induced by the inte-

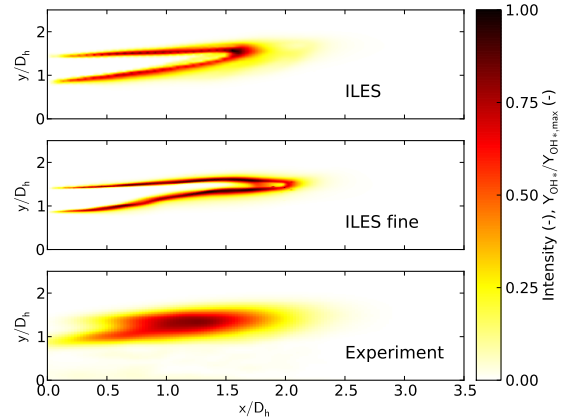


Figure 8: Comparison of the LES with OH\* chemiluminescence measurements ( $\Omega = 0.0$ ,  $\Phi = 0.5$ ,  $T_u = 293$  K). Top and middle: Slices of the normalized OH\* mass fractions (LES), Bottom: Processed Abel inversion of OH\* recordings (Exp.).

Nevertheless, both simulations show a good agreement to the measurements.

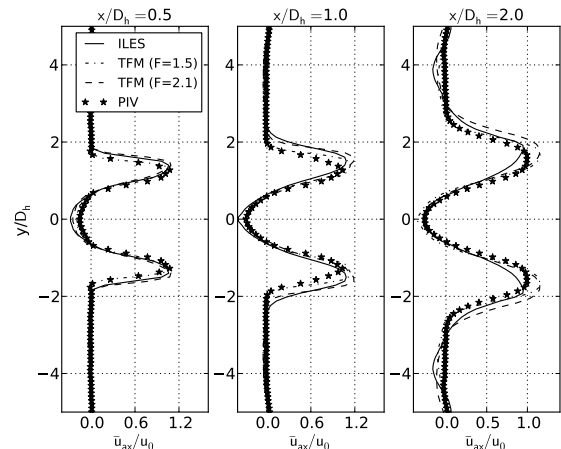


Figure 9: Mean axial and radial velocity profiles at different streamwise positions ( $x/D_h = 0.5; 1.0; 2.0$ ) normalized by the burner exit velocity  $u_0$ .

gration through the line of sight. The algorithm was discussed in detail in [23]. Figure 8 shows the deconvoluted  $\text{OH}^*$  chemiluminescence recordings as well as streamwise slices of  $\text{OH}^*$  mass fraction of the LES. The LES predicts a non-reacting jet surrounded by a thin reaction layer with a steep gradient. The maximum  $\text{OH}^*$  concentration is located at the tip of the reaction layer, contrary to what is observed in the experiments. Compared to the computations the experiments show a shorter jet that leads to a more distributed main reaction zone with a weaker gradient. For the measurements as well as for the computations an area of low  $\text{OH}^*$  concentration is located downstream of the thin reaction layer, which is probably caused by convection. Due to the very small reaction layer thickness, the spatial resolution of the  $\text{OH}^*$  recordings is probably too low to resolve the gradients sufficiently. Nevertheless, the thin flame zone is in line with the previously presented findings, but could be affected by higher mixing. Compared to the coarse case the simulation for the finer grid offers a thinner reaction layer. However, the flame shape and dimension is well represented by the computations. Due to the fact, that both grids showed similar results, the coarser mesh will be used for the following investigations.

To assess the influence of the combustion closure two additional simulations were carried out employing the Thickened Flame Model with  $F = 1.5$  and  $F = 2.1$ . For  $F = 1$  the TFM is formally identical to the ILES closure, which is therefore also shown. Figure 9 shows the mean axial velocity for the computations compared to the experimental data. The highest differences appear in the shear-layer and the inner recirculation zone. But as can be seen all computations are well in line with the experiments.

The Sobel filtered PIV and the accordingly processed computations are given in Figure 10. With increasing  $F$  the flame gets slightly sharper and the flame tip moves closer to the combustor wall. By artificially thickening the flame, the flame seems to be more affected by the convection of the inner shear-layer and the flame extends further downstream. This behavior can also be observed in Figure 11 where  $\text{OH}^*$  chemiluminescence recordings as well as a streamwise slices of  $\text{OH}^*$  mass fraction of the simulations are shown. There the reaction zone is more distributed and extends further downstream. With decreasing  $F$  the flame gets closer to the measurements and for agrees best for values of  $F$  close to unity, which is formally identical to the ILES formulation. In order to gain deeper insight into the combustion process incorporating the dilution of steam the ILES model is employed.

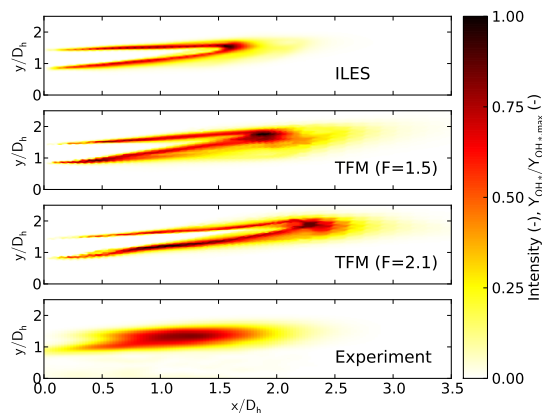


Figure 11: Comparison of the LES with  $\text{OH}^*$  chemiluminescence measurements ( $\Omega = 0.0$ ,  $\Phi = 0.5$ ,  $T_u = 293 \text{ K}$ ). Top to middle: Slices of the normalized  $\text{OH}^*$  mass fractions (LES), Bottom: Processed Abel inversion of  $\text{OH}^*$  recordings (Exp.).

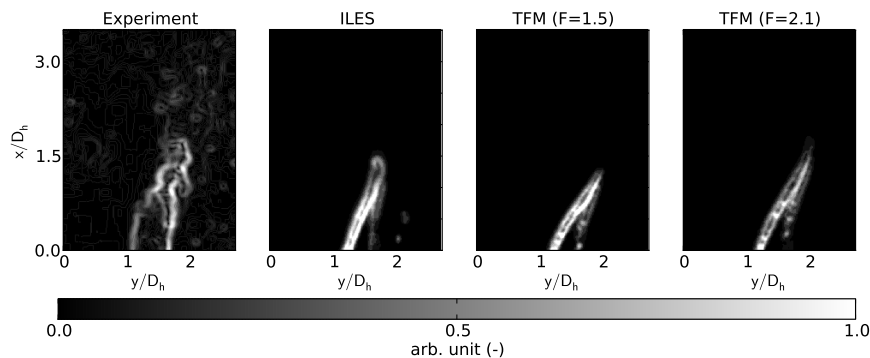


Figure 10: Visualization of the flame front. Processed PIV (left); Inverse temperature gradient of LES (middle to right)

## Influence of Steam

In order to investigate the influence of steam on hydrogen oxidation three simulations with different steam content  $\Omega$  were conducted. The first case was carried out without steam, the second case with moderate steam content ( $\Omega = 20\%$ ) and the last at ultra-wet conditions ( $\Omega = 50\%$ ). For all cases the adiabatic flame temperature was kept constant.

Figure 12 depicts the mean axial velocity for all three cases. As aforementioned in the sensitivity analysis, a inner recirculation zone is established confined by a shear-layer. For the wet cases, a flat velocity profile in the inner recirculation zone can be observed. If the changing of the profile shape can be attributed to higher inlet temperature of the wet case resulting in higher velocities only, remains questionable. The overall predictions of the LES are well in line with the experimental data.

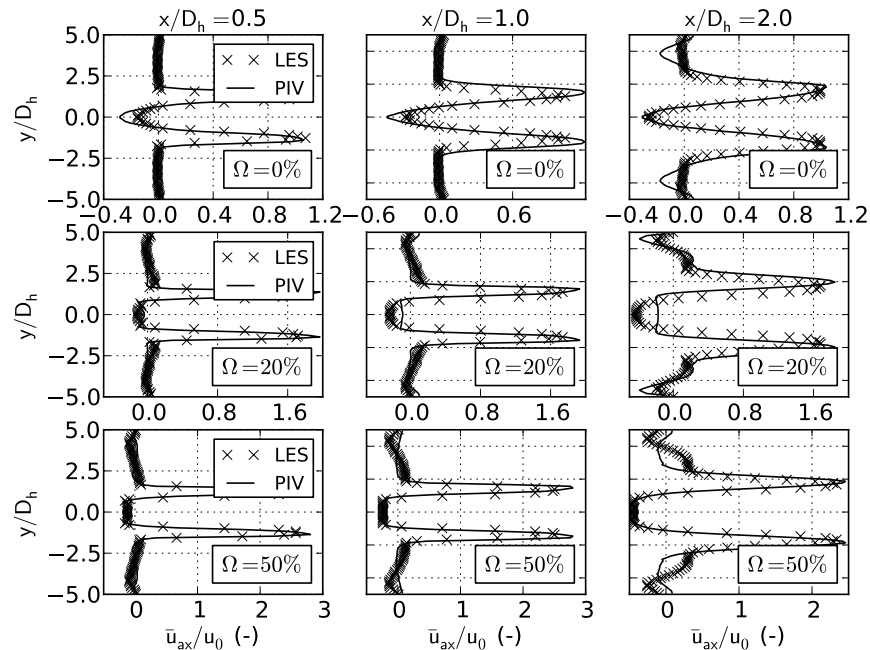


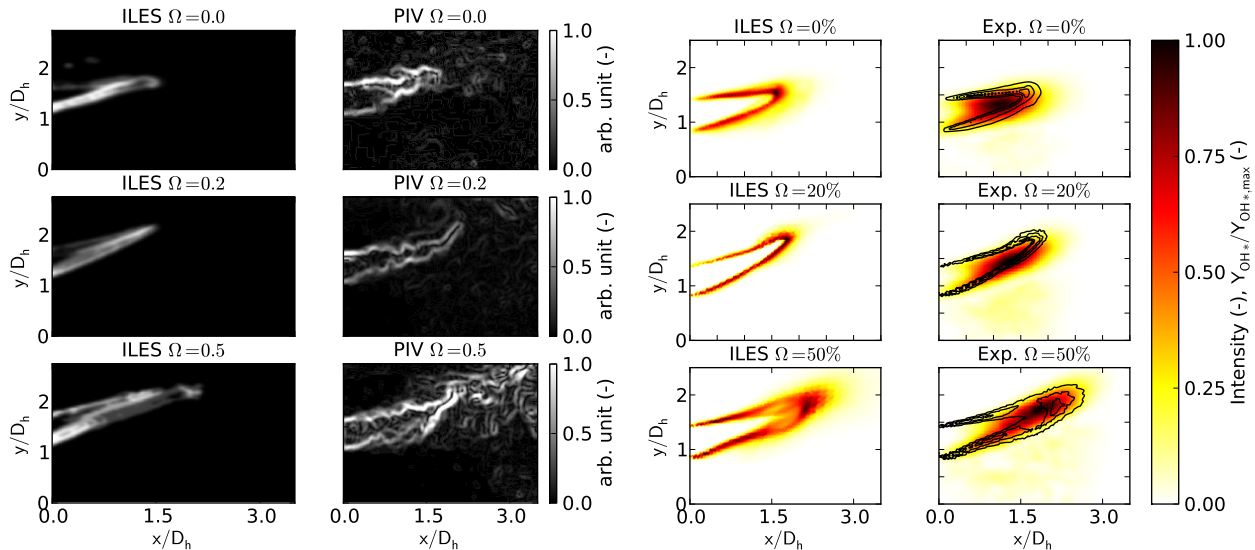
Figure 12: Mean axial velocity profiles at different streamwise positions ( $x/D_h = 0.5; 1.0; 2.0$ ) for different steam levels normalized by the burner exit velocity  $u_0$ .

In Figure 13(a) is the Sobel detected flame front given. The experiments show, that with raising steam content the flame is more influenced by turbulent fluctuations and becomes more wrinkled. Moreover, the figure depicts, that the flame extends further downstream. The simulations reproduce the same trend. As seen before in the sensitivity analysis the wrinkling is not predicted. However, the length, angle and dimensions are well represented.

Figure 13(b) shows a similar behavior. The computations show a larger spatial distributed reaction zone, with a gradient that is less steep, therefore, it can be deduced that the heat release spreads. This increase is well in line with the findings of the kinetical assessment. The prediction of the position of the maximum heat release is in close agreement with the experiments. Moreover, the computations of the flame shape and distribution agree well with the measurements.

To get an impression of the flame dynamics an iso-volume of the  $\text{OH}^*$  mass fraction is shown for the ultra-wet case in Figure 14. The figure shows three perspectives and the flame is colored by the normalized axial velocity fluctuations. As can be seen in the bottom right view, the flame consists of a rapid cold jet, which is surrounded by low velocity fluctuations. Further downstream the flow accelerates and the fluctuation level raises. Also the swirling of the flame can nicely be seen.

Even if the modeling approach presented in this study leads to reasonable results, some limitations should be discussed. For the dry case, the prediction of the distribution of the reaction zone differs slightly between the measurements and the computations. We assume that the spatial resolution of the applied  $\text{OH}^*$  chemi-



(a) Visualization of the flame front. Inverse temperature gradient of LES (left); Processed PIV (right).

(b) Comparison of the LES with OH\* chemiluminescence measurements. Left: Slices of the normalized OH\* mass fractions (LES), Right: Processed Abel inversion of OH\* recordings (Exp.). Contour lines of the OH\* concentration (mass fraction) of the LES are superimposed.

Figure 13: Flame characteristics at different steam dilution levels ( $\Omega = 0.0$ ;  $0.2$ ;  $0.5$ ).

luminescence measurement technique is not high enough to capture the fine structures. Probably, this effect is further amplified by the Abel deconvoluted processing.

However, the velocity field predictions as well as the flame shape and dimension agree well with the experiments. The comparison showed that the detailed mechanism of Burke is suitable to predict steam diluted hydrogen flames under atmospheric gas turbine conditions in terms of inlet temperature. By adding steam to the combustion process, the flame becomes less compact and extends further downstream. Even with high steam content, the extension is small compared to methane flames, as observed in [28, 29].

## 9 Concluding Remarks

This paper contributes to the understanding of the combustion of hydrogen at ultra-wet conditions applying LES. The effect of steam on the combustion process was addressed using detailed chemistry.

In order to identify an adequate oxidation mechanism, several candidates were compared. In particular, their performance was assessed employing one-dimensional laminar premixed flame calculations under dry and wet conditions where experimentally determined flame speeds are available. Out of several reaction models, it was found that the recently published mechanism of Burke was the most suitable. By employing this mechanism further insight into the effect of steam dilution was gained.

In a second step, the mechanism was used for simulating a turbulent flame in a generic swirl burner fed with hydrogen and humidified air. The simulations of the reacting flow were conducted under atmospheric conditions and the steam-air ratio was varied between 0% and 50%. In order to resolve wet combustion, two combustion closures, namely the Implicit Large Eddy Simulation (ILES) and the Thickened Flame Model (TFM) were compared. It was found that the ILES and the TFM with a flame thickening factor close to unity were able to capture the velocity field and flame shape/positions compared to experimental data. For higher values of the flame thickening factor the flame front is stronger influenced by the velocity field. Thus, the reaction zone is further distributed and the the flame angle is tilted closer to the combustion chamber walls.

It was shown that by adding steam, the heat release spreads, the flame front thickens and the flame extends slightly further downstream. Moreover, the velocity fields predicted by the computations were well

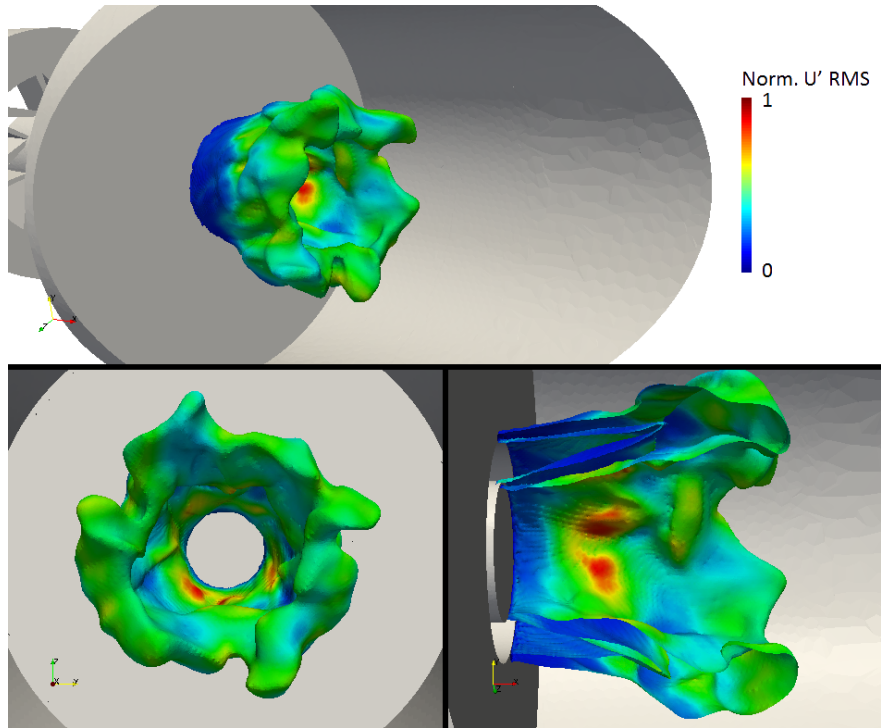


Figure 14: Visualization of the flame dynamics for the ultra-wet case ( $\Omega = 0.5$ ,  $\Phi = 0.75$ ,  $T_{in} = 673$  K). The structure is represented by an iso-volume of  $\text{OH}^*$  and colored by the normalized axial velocity fluctuations.

in line with the measurements. The flame shape and positions agreed well for both the dry and the wet case.

Finally, it was shown that LES is able to recover the flow field. Moreover, by employing a detailed reaction scheme for LES, we were able to predict the flame shape and positions as well as the effects induced by adding steam. The bottom line of this survey is that the addition of steam allows for clean and efficient combustion of hydrogen for gas turbine applications and can be predicted using ILES in combination with detailed chemistry.

## 10 Acknowledgment

The authors would like to thank the CONFET members for fruitful discussions. A part of the computations have been performed at North-German Supercomputing Alliance (HLRN) facilities within the allocation program “Nasse Verbrennung”. The research leading to these results has received funding from the European Research Council under the ERC grant agreement  $n^\circ$  247322, GREENEST.

## References

- [1] A. Bhargava, M. Colket, W. Sowa, K. Casleton, and D. Maloney. An Experimental and Modeling Study of Humid Air Premixed Flames. *Journal of Engineering for Gas Turbines and Power*, 122:405–411, 2000.
- [2] S. Göke, K. Göckeler, O. Krüger, and C. O. Paschereit. Computational and Experimental Study of Premixed Combustion at Ultra Wet Conditions. *Proceedings of ASME Turbo Expo 2010*, (GT2010-23417):1–11, 2010.
- [3] M. Jonsson and J. Yan. Humidified gas turbine - a review of proposed and implemented cycles. *Energy*, 30:1013–1078, 2005.
- [4] M. Bianco, S. M. Camporeale, and B. Fortunato. CFD Simulation of Humid Air Premixed Flame

- Combustion Chamber for Evaporative Gas Turbine Cycles. In *Proceedings of ASME TURBO EXPO 2001*, 2001.
- [5] P. Guo, S. Zang, and B. Ge. LES and Experimental Study of Flow Features in Humid-Air Combustion Chamber with Non-Premixed Circular-disc Stabilized Flames. In *Proceedings of ASME Turbo Expo 2008: Power for Land, Sea and Air*, 2008.
- [6] M. Ó Conaire, H. J. Curran, J. M. Simmie, W. J. Pitz, and C. K. Westbrook. A comprehensive modeling study of hydrogen oxidation. *International Journal of Chemical Kinetics*, 36(11):603–622, November 2004.
- [7] D. Dowdy. The use of expanding spherical flames to determine burning velocities and stretch effects in hydrogen/air mixtures. *Symposium (International) on Combustion*, 23(1):325–332, 1991.
- [8] S. D. Tse, D. L. Zhu, and C. K. Law. Morphology and burning rates of expanding spherical flames in H<sub>2</sub>/O<sub>2</sub>/inert mixtures up to 60 atmospheres. *Proceedings of the Combustion Institute*, 28(2):1793–1800, January 2000.
- [9] W. T. David and J. Mann. Influence of Water Vapour on Flame Gas Temperatures. *Nature*, 150(3809):521–522, October 1942.
- [10] D. K. Kuehl. Effects of water on burning velocity of hydrogen-air flames. *American Rocket Society Journal*, 32:1724–1726, 1962.
- [11] A. Levy. Effects of Water on Hydrogen Flames. *AIAA Journal*, 1(5):1239–1239, May 1963.
- [12] G. Dixon-Lewis and A. Williams. The rate of heat release in some slow burning hydrogen-oxygen flames. *Combustion and Flame*, 8(4):249–255, December 1964.
- [13] D. Liu and R. MacFarlane. Laminar burning velocities of hydrogen-air and hydrogen-air-steam flames. *Combustion and Flame*, 49(1-3):59–71, 1983.
- [14] G. W. Koroll and S. R. Mulpuru. The effect of dilution with steam on the burning velocity and structure of premixed hydrogen flames. *Symposium (International) on Combustion*, 21(1):1811–1819, 1988.
- [15] O. C. Kwon and G. M. Faeth. Flame/stretch interactions of premixed hydrogen-fueled flames: measurements and predictions. *Combustion and Flame*, 124(4):590–610, March 2001.
- [16] M. Kuznetsov, R. Redlinger, W. Breitung, J. Grune, a. Friedrich, and N. Ichikawa. Laminar burning velocities of hydrogen-oxygen-steam mixtures at elevated temperatures and pressures. *Proceedings of the Combustion Institute*, 33(1):895–903, 2011.
- [17] J. Ströhle and T. Myhrvold. An evaluation of detailed reaction mechanisms for hydrogen combustion under gas turbine conditions. *International Journal of Hydrogen Energy*, 32(1):125–135, January 2007.
- [18] Juan Li, Zhenwei Zhao, Andrei Kazakov, and Frederick L. Dryer. An updated comprehensive kinetic model of hydrogen combustion. *International Journal of Chemical Kinetics*, 36(10):566–575, October 2004.
- [19] M. P. Burke, M. Chaos, Y. Ju, F. L. Dryer, and S. J. Klippenstein. Comprehensive H<sub>2</sub>/O<sub>2</sub> kinetic model for high-pressure combustion. *International Journal of Chemical Kinetics*, pages 1–68, December 2012.
- [20] T. Le Cong and P. Dagaut. Oxidation of H<sub>2</sub>/CO<sub>2</sub> mixtures and effect of hydrogen initial concentration on the combustion of CH<sub>4</sub> and CH<sub>4</sub>/CO<sub>2</sub> mixtures: Experiments and modeling. *Proceedings of the Combustion Institute*, 32(1):427–435, 2009.
- [21] A. Frassoldati, T. Faravelli, and E. Ranzi. The ignition, combustion and flame structure of carbon monoxide/hydrogen mixtures. Note 1: Detailed kinetic modeling of syngas combustion also in presence of nitrogen compounds. *International Journal of Hydrogen Energy*, 32(15):3471–3485, October 2007.
- [22] S. Göke, S. Terhaar, S. Schimek, G. Katharina, and C. O. Paschereit. Combustion of Natural Gas, Hydrogen And Bio-Fuels at Ultra-Wet Conditions. *Proceedings of ASME Turbo Expo 2011*, GT2011-456, 2011.
- [23] S. M. Jaffe, J. Larjo, and R. Henberg. Abel Inversion Using the Fast Fourier Transform. In *10th International Symposium on Plasma Chemistry*, 1991.
- [24] S. Terhaar, K. Göckeler, S. Schimek, S. Göke, and C. O. Paschereit. Non-Reacting and Reacting Flow in a Swirl-Stabilized Burner for Ultra-Wet Combustion. In *41st AIAA Fluid Dynamics Conference and Exhibit, 27-30 June 2011, Honolulu, Hawaii*, number AIAA 2011-3584, 2011.
- [25] T. Poinsot and D. Veynante. *Theoretical and Numerical Combustion*. R T Edwards Inc, 2nd edition, 2005.
- [26] H. G. Weller, G. Tabora, and H. Jasak. A tensorial approach to computational continuum mechanics

- using object-oriented techniques. *Computers in Physics*, 12(6):620–631, 1998.
- [27] J. Smagorinsky. General circulation experiments with the primitive equations, I. the basic experiment. *Monthly Weather Review*, 91(3):99–164, 1963.
- [28] O. Krüger, C. Duwig, S. Göke, K. Göckeler, S. Terhaar, C. O. Paschereit, and L. Fuchs. Numerical Investigations of a Swirl-stabilized Premixed Flame at Ultra-Wet Conditions. *Proceedings of ASME Turbo Expo 2011*, (GT2011-45866):1–12, 2011.
- [29] O. Krüger, C. Duwig, S. Göke, C. O. Paschereit, and L. Fuchs. Large Eddy Simulation of Ultra-Wet Premixed Flames for Gas Turbine Applications. In *Proceedings of the European Combustion Meeting 2011*, pages 1–6, 2011.
- [30] O. Krüger, C. Duwig, S. Terhaar, and C. O. Paschereit. Large Eddy Simulations of Hydrogen Oxidation at Ultra-wet Conditions in a Model Gas Turbine Combustor Applying Detailed Chemistry. *Proceedings of ASME Turbo Expo 2012*, (GT2012-69446), 2012.
- [31] R. I. Issa. Solution of the implicitly discretized fluid flow equations by operator-splitting. *Journal of Computational Physics*, 62:40–65, 1986.
- [32] G. P. Smith, D. M. Golden, M. Frenklach, N. W. Moriarty, B. Eiteneer, M. Goldenberg, C. T. Bowman, R. K. Hanson, S. Song, W. C. Jr. Gardiner, V. V. Lissianski, and Z. Qin. *GRI 3.0*. [http://www.me.berkeley.edu/gri\\_mech/](http://www.me.berkeley.edu/gri_mech/), 2000.
- [33] G. P. Smith, J. Luque, C. Park, J. B. Jeffries, and D. R. Crosley. Low pressure flame determinations of rate constants for OH(A) and CH(A) chemiluminescence. *Combustion and Flame*, 131(1-2):59–69, October 2002.
- [34] C. Fureby. Comparison of Flamelet and Finite Rate Chemistry LES for Premixed Turbulent Combustion. *45th AIAA Aerospace Sciences Meeting and Exhibit*, (AIAA 2007-1413):1–16, 2007.
- [35] C. Duwig and E. Gutmark. Large scale rotating motions in a multiple jets combustor. *Physics of Fluids*, 20(4):41705, 2008.
- [36] C. Duwig, K.-J. Nogenmyr, C. Chan, and M. J. Dunn. Large Eddy Simulations of a piloted lean premix jet flame using finite-rate chemistry. *Combustion Theory and Modelling*, 15(4):537–568, August 2011.
- [37] T. D. Butler and P. J. O’Rourke. A Numerical Method for Two Dimensional Unsteady Reacting Flows. *Symposium (International) on Combustion*, 16(1):1503–1515, 1977.
- [38] L. Selle, G. Lartigue, T. Poinso, R. Koch, K.-U. Schildemacher, W. Krebs, B. Prade, P. Kaufmann, and D. Veynante. Compressible large eddy simulation of turbulent combustion in complex geometry on unstructured meshes. *Combustion and Flame*, 137:489–505, 2004.
- [39] B. A. Sen and S. Menon. Linear eddy mixing based tabulation and artificial neural networks for large eddy simulations of turbulent flames. *Combustion and Flame*, 157:62–74, 2010.
- [40] C. Duwig, L. Fuchs, P. Griebel, P. Siewert, and E. Boschek. Study of a Confined Turbulent Jet: Influence of Combustion and Pressure. *AIAA Journal*, 45(3):624–639, March 2007.
- [41] C. Duwig and L. Fuchs. Study of Flame Stabilization in a Swirling Combustor Using a New Flamelet Formulation. *Combustion Science and Technology*, 177:1485, 2005.
- [42] H. Pitsch and L. de Lageneste. Large-Eddy Simulation of Premixed Turbulent Combustion Using a Level-Set Approach. *Proceedings of the Combustion Institute*, 29:2001–2008, 2003.
- [43] E. Giacomazzi and V. Battaglia. The coupling of turbulence and chemistry in a premixed bluff-body flame as studied by LES. *Combustion and Flame*, 134-4:320–335, 2004.
- [44] S. Raman and H. Pitsch. A consistent LES/filtered-density function formulation for the simulation of turbulent flames with detailed chemistry. *Proceedings of the Combustion Institute*, 31:1711–1719, 2007.
- [45] F. Grinstein and K. Kailasanath. Three Dimensional Numerical Simulations of Unsteady Reactive Square Jets. *Combustion and Flame*, 100:2–10, 1994.
- [46] G. M. Goldin. Evaluation of LES subgrid reaction models in a lifted flame. *43rd AIAA Aerospace Sciences Meeting and Exhibit, Reno*, page 555, 2005.
- [47] O. Colin, F. Ducros, D. Veynante, and T. Poinso. A thickened flame model for large eddy simulations of turbulent premixed combustion. *Physics of Fluids*, 12(7):1843, 2000.
- [48] J. P. Legier, T. Poinso, and D. Veynante. Dynamically thickened flame LES model for premixed and non-premixed turbulent combustion. *Proc. of the summer program*, pages 157–168, 2000.
- [49] C. Fureby. A fractal flame-wrinkling large eddy simulation model for premixed turbulent combustion. *Proceedings of the Combustion Institute*, 30(1):593–601, January 2005.
- [50] O. Krüger, C. Duwig, K. Göckeler, S. Terhaar, C. Strangfeld, C. O. Paschereit, and L. Fuchs. Identifi-

- cation of Coherent Structures in a Turbulent Generic Swirl Burner using Large Eddy Simulations. *20th AIAA Computational Fluid Dynamics Conference*, (AIAA 2011-3549):1–14, 2011.
- [51] S. Terhaar, B. C. Bobusch, and C. O. Paschereit. Effects of Outlet Boundary Conditions on the Reacting Flow Field in a Swirl-Stabilized Combustor at Dry and Humidified Conditions. *Proceedings of ASME Turbo Expo 2012*, GT2012-697, 2012.
- [52] H. Edmondson and M.P. Heap. The burning velocity of hydrogen-air flames. *Combustion and flame*, 16(2):161–165, 1971.
- [53] M. P. Burke, M. Chaos, Y. Ju, F. L. Dryer, and S. J. Klippenstein. Comprehensive H<sub>2</sub>/O<sub>2</sub> Kinetic Model for High-Pressure Combustion. *International Journal of Chemical Kinetics*, (in press):1–135, 2011.
- [54] G. P. Smith, C. Park, and J. Luque. A note on chemiluminescence in low-pressure hydrogen and methane-nitrous oxide flames. *Combustion and Flame*, 140(4):385–389, March 2005.
- [55] S. Pfadler, F. Beyrau, and A. Leipertz. Flame front detection and characterization using conditioned particle image velocimetry (CPIV). *Optics Express*, 81(1-2):205–219, August 2007.
- [56] S. Tachibana, L. Zimmer, and S. Kazuo. Flame front detection and dynamics using PIV in a turbulent premixed flame. *12th International Symposium on Applications of Laser Techniques to Fluid Mechanics*, 2004.